Dalton Transactions

ROYAL SOCIETY OF CHEMISTRY

PAPER

View Article Online
View Journal | View Issue

Cite this: *Dalton Trans.*, 2026, **55**, 165

Catalytic oxidative coupling of methane over mixed-anion rare-earth oxyfluorides: composition/structure–activity relationships

Afif Pamungkas, [a] Takumi Kaga,[a] Kosaku Ohishi, [a] Satoshi Ogawa, [a] Miwa Saito, [a] Satoshi Ishikawa, [b] Wataru Ueda [a] and Teruki Motohashi *[a]

The incorporation of fluoride anions into oxide catalysts can modify their structural and surface properties, consequently influencing their catalytic performance. In this work, a series of rare-earth oxyfluorides (REOF; RE = La, Sm, Eu, Dy, Y, and Yb) was investigated for their catalytic activity in the oxidative coupling of methane (OCM). All REOFs crystallize in a trigonal structure, except YbOF, which adopts either monoclinic (YbOF-m) or tetragonal (YbOF-t) polymorphs. The CH_4 conversion and C_2 selectivity on the REOF catalysts at 600 and 800 °C exhibit systematic increasing or decreasing trends that correlate with the ionic radii of the RE^{3+} cations. Among the trigonal REOFs, YOF shows the highest CH_4 conversion and C_2 selectivity at 800 °C, with values of 24.8% and 44.9%, respectively. CO_2- and O_2-temperature-programmed desorption (TPD) analyses reveal that OCM activity, lattice size, basicity, and surface oxygen species follow similar trends, indicating correlations among these factors. Larger lattice parameters and longer RE-(O,F) bond lengths are associated with a higher density of moderate basic sites and moderately bound surface oxygen species. Finally, YbOF-m exhibits superior CH_4 conversion and C_2 selectivity compared to its tetragonal polymorph, YbOF-t. At 700 °C, the C_2 selectivities are 45.2% and 14.5% for the monoclinic and tetragonal phases, respectively.

Received 21st October 2025,
Accepted 17th November 2025

DOI: 10.1039/d5dt02519b

rsc.li/dalton

Introduction

Methane is a promising feedstock for chemical synthesis owing to its low cost and abundant availability in natural gas. It possesses the highest hydrogen-to-carbon ratio among hydrocarbons, making it an attractive source of hydrogen fuels and hydrogen-rich chemicals.[1] Despite these advantages, methane remains underutilized because it is primarily combusted for electricity and heat generation or flared during oil extraction.[2] Consequently, further research, particularly in catalyst development, is required to enhance the efficiency of methane utilization.

In industrial processes, methane conversion typically proceeds *via* an indirect route: methane is first reformed into syngas, which is subsequently transformed into other chemicals.[3] However, this multistep process is economically inefficient, and therefore, a more straightforward route to methane conversion is desirable. Such an approach would not only improve energy efficiency but also reduce carbon emissions associated with conventional reforming pathways.[4] To this end, extensive research has focused on direct methane conversion, with reports describing the production of methanol, formaldehyde, and acetic acid.[5–7] In addition to oxygenates, methane can also be converted into olefins and aromatics.[8]

The oxidative coupling of methane (OCM) converts methane into higher hydrocarbons (C_2 species), primarily ethane (eqn (1)) and ethylene (eqn (2)), the latter of which is a key feedstock for chemical and polymer syntheses.[9] Despite extensive efforts to design catalysts with high yields, satisfactory results have not yet been achieved. Methane is a highly stable molecule with strong C–H bonds, making its activation particularly challenging. In addition, CO_x byproducts are thermodynamically favorable and form more rapidly, thereby reducing C_2 selectivity. Among the reported catalysts,[10] a composite consisting of manganese oxides and sodium tungstates on a silica support, denoted as Mn-Na_2WO_4/SiO_2, is considered state-of-the-art because of its high yield and stability.[11,12] However, the origin of its activity remains under debate due to its complex structure.[13] Another frequently investigated OCM catalyst class is alkaline earth oxides. Previous studies have shown that catalyst basicity plays a critical role in methane adsorption and activation,[14,15] and alkaline earth oxides exhibit relatively high basicity. Basic sites

[a]*Department of Applied Chemistry, Faculty of Chemistry and Biochemistry, Kanagawa University, Yokohama 221-8686, Japan. E-mail: t-mot@kanagawa-u.ac.jp*
[b]*Materials and Structures Laboratory, Institute of Integrated Research, Institute of Science Tokyo, Yokohama 221-8501, Japan*

facilitate the formation of methyl radicals, the active species in the OCM reaction. Rare earth oxides (REOs) are also highly active OCM catalysts owing to their abundant basic sites. For instance, La_2O_3 and Sm_2O_3 are among the most active lanthanide catalysts and have therefore been extensively studied.[3,16–18]

$$2CH_4 + 1/2O_2 \rightarrow C_2H_6 + H_2O \quad (1)$$

$$2CH_4 + O_2 \rightarrow C_2H_4 + 2H_2O \quad (2)$$

Previous studies have reported that alkaline and alkaline earth metal halides can enhance C_2 selectivity. Xi *et al.* investigated the promotional effect of barium halides on SnO_2 for OCM and observed the enhanced activity upon halide incorporation. They concluded that barium halides generate more OCM selective oxygen sites and moderate basic sites.[19] Similar positive effects of barium halides have also been observed for other catalysts such as La_2O_3, $BaSnO_3$, and Gd_2O_3.[20–22] Long *et al.* reported that SrF_2 doping into Y_2O_3 decreases both acidity and basicity but improves the activity of Y_2O_3.[23] Cheng *et al.* demonstrated that chloride ions improve the activity of Li/SnO_2 catalysts by increasing anion vacancy concentrations and enhancing oxygen mobility, thereby strengthening the redox ability of Sn.[24] Hiyoshi *et al.* revealed that alkali chloride-promoted $Mn\text{-}Na_2WO_4/SiO_2$ exhibits higher methane conversion and ethylene selectivity.[25] Furthermore, Au *et al.* studied OCM activity over a LaF_3/La_2O_3 catalyst and proposed LaOF as the active phase.[26] Collectively, these results indicate that the incorporation of halide anions and their interaction with oxide anions exerts beneficial effects on OCM activity.

Rare-earth oxyfluorides (REOFs) are mixed-anion rare-earth compounds that exhibit unique properties arising from the coexistence of multiple anion species. For instance, REOFs display high optical transparency and low phonon energy, making them suitable as host matrices for fluorescent materials.[27] In addition, REOFs exhibit higher thermal stability under oxygen atmospheres compared to their corresponding fluorides.[28] Their ionic conductivity is also tunable depending on the O/F ratio,[29] which is of interest for applications in electrochemical devices, and has already been exploited in several catalyst studies.[30,31] With respect to OCM catalysis, Au *et al.* reported OCM activity for LaOF;[32] however, no comprehensive investigation of the REOF family has been conducted, and thus, the catalytic activity trends of REOFs remain unknown.

Herein, we investigated a series of REOFs with RE = La, Sm, Eu, Dy, Y, and Yb. The REOF phases with RE = La, Sm, Eu, Dy, and Y crystallize in a trigonal structure, whereas YbOF adopts either a monoclinic (YbOF-m) or tetragonal (YbOF-t) phase, as reported previously.[28,29] In this study, we focus on the OCM activity of single-phase oxyfluorides rather than oxide-fluoride composites, as the former provide atomic-level chemical uniformity and well-defined active sites, making them suitable for fundamental investigations.[33] The objective of this work is to elucidate the effects of fluoride anions on the REOF crystal structure, surface properties, and OCM catalytic activity, and to uncover the catalytic potential of the REOF family.

Experimental

Material synthesis

The following chemicals were used as starting reagents: Y_2O_3 (FUJIFILM Wako Chemicals, 99.99%), YF_3 (Kanto Chemical, 99.99%), La_2O_3 (High Purity Chemicals, 99.99%), LaF_3 (High Purity Chemicals, 99.9%), Sm_2O_3 (FUJIFILM Wako Chemicals, 99.9%), SmF_3 (Mitsuwa's Pure Chemicals, 99.9%), Eu_2O_3 (High Purity Chemicals, 99.9%), EuF_3 (Mitsuwa's Pure Chemicals, 99.9%), Dy_2O_3 (High Purity Chemicals, 99.9%), DyF_3 (Mitsuwa's Pure Chemicals, 99.9%), Yb_2O_3 (High Purity Chemicals, 99.9%), YbF_3 (Mitsuwa's Pure Chemicals, 99.9%), and NH_4F (FUJIFILM Wako Chemicals). For REOFs with RE = La, Sm, Eu, Dy, and Y, the corresponding oxides and fluorides were ground in an agate mortar until homogeneous. The mixtures were transferred to a tubular furnace and fired at 800 °C under an air flow for 12 h.[29] YbOF-t was obtained from a mixture of Yb_2O_3 and NH_4F, heated at 970 °C under a N_2 flow for 12 h. YbOF-m was prepared following a previously reported procedure.[34] A mixture of Yb_2O_3 and YbF_3 was heated at 950 °C under a N_2 flow for 24 h, followed by successive post-annealing steps at decreasing temperatures down to 400 °C for a total duration of one week.

The phase purity of the samples was examined by X-ray powder diffraction (Rigaku Ultima IV, Cu-Kα radiation). Elemental homogeneity and chemical composition of the samples were analyzed using a scanning electron microscope (SEM; Hitachi High-Tech SU-5000) equipped with an energy-dispersive X-ray spectrometer (EDS; Bruker XFlash Detector 630M). Nitrogen adsorption/desorption isotherms were measured at 77 K using BELSORP-mini II (Microtrac). Prior to measurement, the samples were pretreated at 300 °C under vacuum and subsequently exposed to N_2. Specific surface areas were calculated using the Brunauer–Emmett–Teller (BET) method.

CO_2 and O_2 adsorption profiles were analyzed using CO_2- and O_2-temperature programmed desorption (TPD), respectively. For each measurement, 0.1 g of sample was pretreated at 800 °C under a He flow, cooled to 100 °C, and subsequently exposed to CO_2 or O_2 flow for 30 min. The system was then purged with He prior to desorption analysis. The sample was heated to 800 °C at a rate of 10 °C min^{-1}, and adsorption curves were recorded using a GC-TCD (GC-3210, GL Sciences).

Catalytic activity tests

Catalytic activity tests were carried out in an alumina tube reactor (inner diameter ≈5 mm) placed inside a tubular furnace. The catalyst bed consisted of 0.30 g of REOFs prepared in this work or commercial REOs as described in the "Material synthesis" section. The REOs were used as received without further treatment. A feed gas mixture containing CH_4 (1 mL min^{-1}), O_2 (0.25 mL min^{-1}), and N_2 (8.75 mL min^{-1})

was passed through the catalyst bed. The temperature was increased to 600 °C and maintained for 20 min to ensure steady-state operation. The effluent gases were analyzed using a GC-TCD (Inficon micro GC) equipped with two columns: molecular sieve 5A and Plot-Q. Methane conversion (X), C_2 selectivity (S), and C_2 yield (Y) were calculated using the following formula. The detectable coupling products were ethane and ethylene; thus, the term C_2 refers to these two products. A blank test of the reactor setup indicated that the temperature rise due to the exothermic OCM reaction was negligible, owing to the small O_2 and CH_4 flow rates.[33]

$$X_{CH_4} = \frac{n_{CH_4\,in} - n_{CH_4\,out}}{n_{CH_4\,in}} \times 100\% \quad (3)$$

$$Y_{C_2} = \frac{n_{C_2}}{n_{CH_4\,in}} \times 100\% \quad (4)$$

$$S_{C_2} = \frac{Y_{C_2}}{X_{CH_4}} \times 100\% \quad (5)$$

Results and discussion

XRD analysis reveals that the REOFs, except for YbOF, crystallize in a trigonal structure (Fig. 1), consistent with the previous report.[29] YbOF is known to adopt two polymorphs, monoclinic (YbOF-m) and tetragonal (YbOF-t).[28] While the REOF samples generally exhibit high phase purity, YbOF-m contains Yb_2O_3 and YbOF-t as impurities. The lattice parameters, summarized in Table S1, follow the expected trend based on the ionic radii of RE cations: Y < Dy < Eu < Sm < La. The XRD patterns and lattice parameters for the spent catalysts were measured after catalytic testing at 800 °C (Fig. S1 and Table S2). No significant changes are observed, except for YbOF-m, which remains stable up to 700 °C but undergoes a phase transformation to YbOF-t at higher temperatures, indicating that the monoclinic phase is metastable above 700 °C. The REOF catalysts, with the exception of YbOF-m, exhibit good chemical stability during OCM tests up to 800 °C. The specific surface areas of REOFs with RE = La, Sm, Eu, Dy, and Y are in the range of 1.47–4.14 $m^2\ g^{-1}$, whereas YbOF-t and YbOF-m exhibit slightly lower values (Table S3). These surface areas are relatively small for catalytic applications and, therefore, expected to exert only a minor influence on catalytic activity.

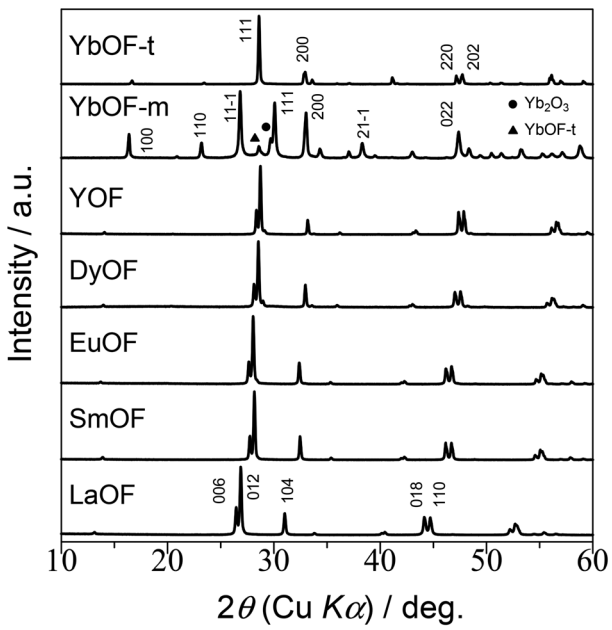

Fig. 1 XRD patterns for LaOF, SmOF, EuOF, DyOF, YOF, YbOF-m, and YbOF-t.

Because YbOF possesses a distinct crystal structure compared to the other REOFs, the following discussion first addresses the REOFs with RE = La, Sm, Eu, Dy, and Y, followed by YbOF.

Fig. 2a–f show the temperature dependence of the OCM activity of the REOF catalysts, with detailed data provided in Tables S4–S10. For all catalysts, the detected carbon products are C_2H_4, C_2H_6, CO, and CO_2. All catalysts exhibit a similar trend in OCM performance; both CH_4 conversion and C_2 selectivity increase with temperature. At 600 °C, the REOFs (RE = La, Sm, Eu, Dy, and Y) display comparable CH_4 conversions (X_{CH_4} = 19–22%) but differing C_2 selectivities (S_{C_2} = 10–20%). Among them, YOF and LaOF demonstrate the lowest and highest C_2 selectivities of 10.8% and 20.1%, respectively. At 800 °C, the CH_4 conversions remain comparable (X_{CH_4} = 23–25%), but the trend in C_2 selectivity is reversed. YOF exhibits the highest C_2 selectivity (S_{C_2} = 44.9%), while LaOF shows the lowest (S_{C_2} = 39.2%). The variations in conversion and selectivity at elevated temperatures suggest a systematic trend, which will be discussed in detail below.

The catalytic activities of the corresponding rare-earth oxides (REOs) were also examined for comparison (Fig. 2a–f). At 600 °C, CH_4 conversions range from X_{CH_4} = 19% to 23%, with the highest and lowest values observed for Yb_2O_3 (23.3%) and Y_2O_3 (19.5%), respectively. Regarding C_2 selectivity, Yb_2O_3 and Eu_2O_3 achieve S_{C_2} > 20% at this temperature, whereas Y_2O_3 exhibits the lowest C_2 selectivity (S_{C_2} = 6.8%). The REO series generally displays a similar trend in C_2 selectivity, with the exception of Eu_2O_3. For this catalyst, selectivity increases to a maximum value of 38.2% at 700 °C before decreasing to 19.3% at 800 °C, approximately half of the maximum value. In addition, La_2O_3 exhibits the highest C_2 selectivity of 46.9% at 750 °C.

The catalytic activity trends of REOFs are highlighted by summarizing the X_{CH_4} and S_{C_2} values at 600 and 800 °C (Fig. 3a and b), with the data arranged in order of increasing ionic radius (eightfold coordination) of Y^{3+} (1.019 Å), Dy^{3+} (1.027 Å), Eu^{3+} (1.066 Å), Sm^{3+} (1.079 Å), and La^{3+} (1.160 Å).[35] The REO data are similarly presented in Fig. 3c and d, but in this case, the catalytic activity trends are less apparent, likely due to the presence of multiple structural types.[36]

The comparison of catalytic activities of REOFs with those of their corresponding REOs reveals several significant findings (Fig. 2a–f). REOFs with a trigonal structure, RE = La, Sm,

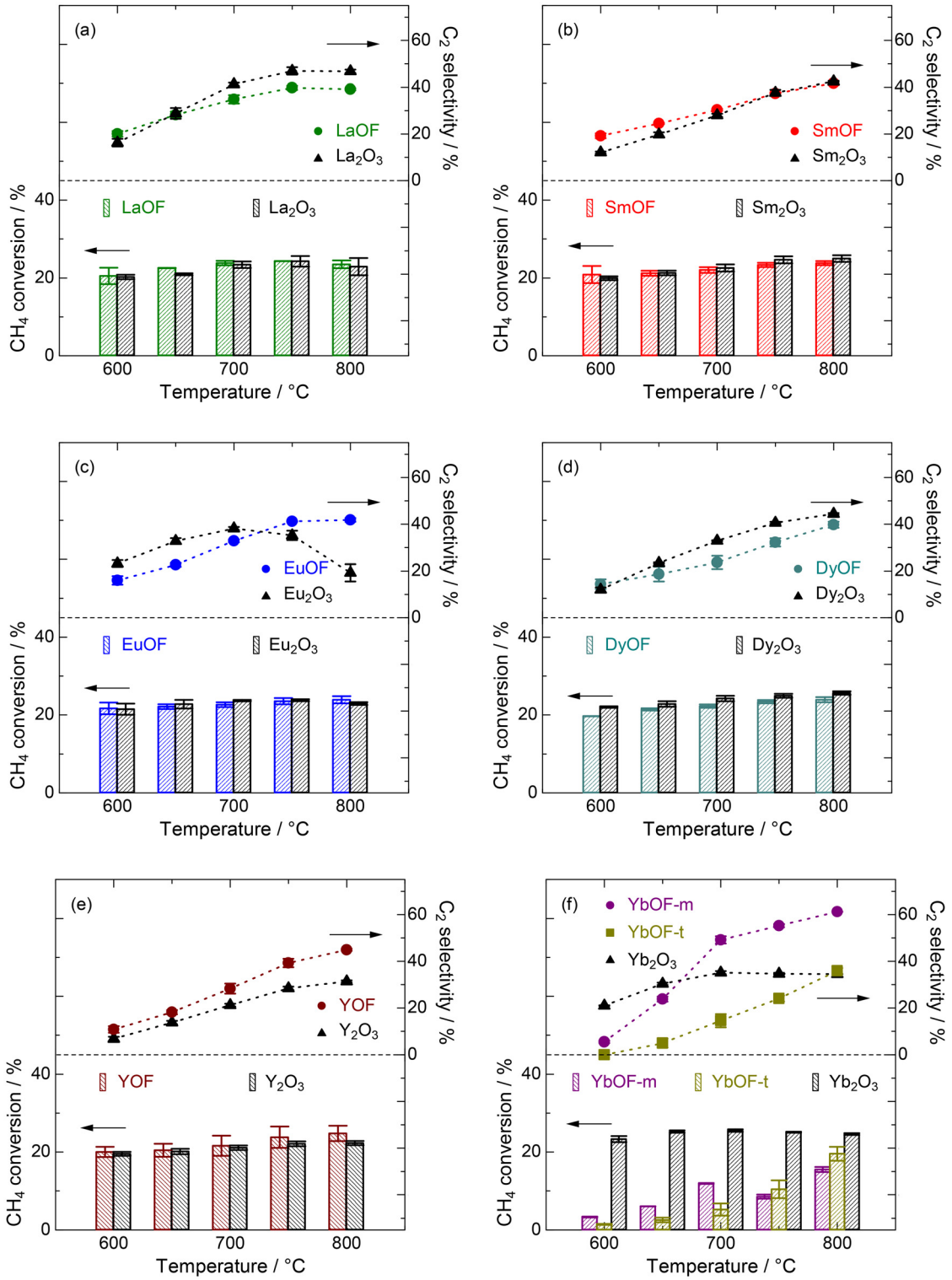

Fig. 2 CH_4 conversions and C_2 selectivities of (a) LaOF, (b) SmOF, (c) EuOF, (d) DyOF, (e) YOF, and (f) YbOF. The data of their corresponding oxides are also presented.

Eu, Dy, and Y, exhibit comparable CH_4 conversions to their respective oxides (Fig. 2 and 3). Notably, among the REOF series, only YOF demonstrates higher C_2 selectivity than its oxide at the entire temperature range (Fig. 2e). At 600 °C, S_{C_2} = 10.8% is approximately twice that of Y_2O_3. The C_2 selectivity of YOF reaches 39.3% and 44.9% at 750 °C and 800 °C, respectively, much higher than S_{C_2} = 31.4% for Y_2O_3 at 800 °C.

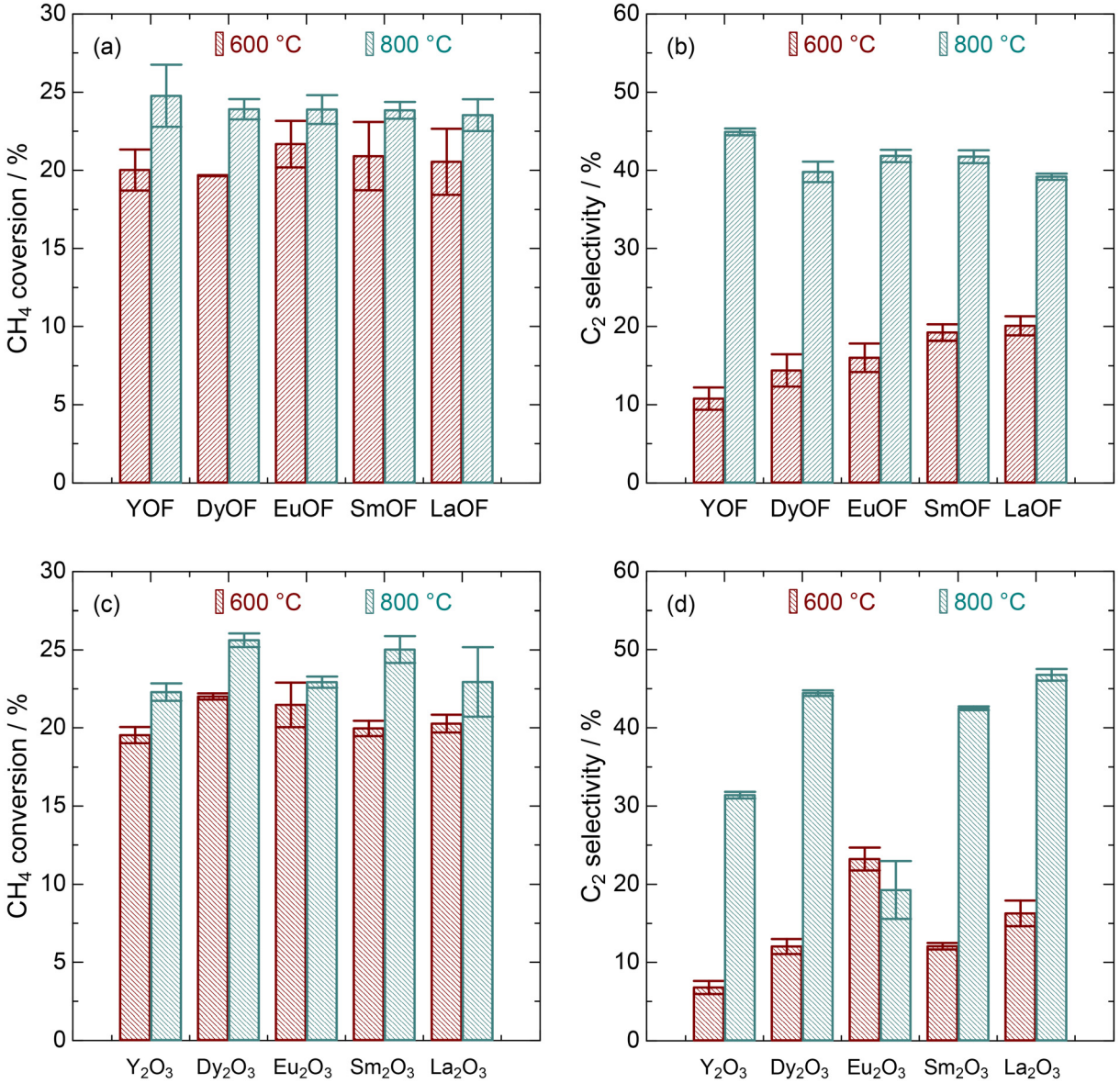

Fig. 3 (a) CH_4 conversions and (b) C_2 selectivities of REOFs at 600 and 800 °C. Those of REOs are plotted in (c) and (d). In each graph, the data are arranged in order of increasing ionic radius of RE^{3+}.

The unusual OCM performance of Eu_2O_3 warrants attention. Although EuOF and Eu_2O_3 exhibit comparable CH_4 conversions across the entire temperature range, their C_2 selectivity behaviors clearly differ (Fig. 2c). For Eu_2O_3, C_2 selectivity decreases above 700 °C, whereas for EuOF it continues to increase, reaching a maximum of 41.8% at 800 °C. Given the similar specific surface areas of Eu_2O_3 (3.97 $m^2\ g^{-1}$) and EuOF (3.39 $m^2\ g^{-1}$), grain morphology is unlikely to be a decisive factor in the anomalous behavior of Eu_2O_3. Instead, the characteristic redox capability of Eu^{2+}/Eu^{3+} cations is proposed to promote deep methane oxidation, which may be suppressed in EuOF owing to the higher electronegativity of fluorine relative to oxygen.

For YbOF, two polymorphs of monoclinic (YbOF-m) and tetragonal (YbOF-t) were successfully obtained. Notably, their OCM performance differs significantly (Fig. 2f), despite their identical nominal compositions. YbOF-t overall exhibits lower CH_4 conversion and C_2 selectivity than Yb_2O_3. At 600 °C, the CH_4 conversion on YbOF-t is very low (X_{CH_4} = 1.4%), and no C_2 products are detected. The maximum values of CH_4 conversion and C_2 selectivity are X_{CH_4} = 19.6% and S_{C_2} = 35.9%, respectively, achieved at 800 °C. In contrast, YbOF-m shows slightly higher activity than YbOF-t at 600 °C, with X_{CH_4} = 3.5% and S_{C_2} = 4.1%. At 700 °C, these values increase markedly to X_{CH_4} = 11.5% and S_{C_2} = 45.2%, both of which are much higher than X_{CH_4} = 5.3% and S_{C_2} = 14.5% for YbOF-t. However, YbOF-m undergoes a phase transformation above ~700 °C; therefore, the data at 700 °C represent the highest observed activity. Importantly, YbOF-m achieves higher C_2 selectivity than Yb_2O_3

and all other REOFs investigated at this temperature. Although the YbOF-m phase disappears at elevated temperatures, C_2 selectivity of the catalyst continues to increase above 700 °C. The decomposition of YbOF-m into YbOF-t and Yb_2O_3 may generate an interface between these phases, resulting in the formation of OCM-selective active sites that enhance C_2 formation. Fig. S2 shows the catalytic activity of YbOF-m and YbOF-t over three consecutive catalytic test cycles. While YbOF-t exhibits stable conversion and selectivity, indicative of its high surface stability, the catalytic activity of YbOF-m progressively decreases in each cycle. The result suggests that the metastable YbOF-m phase transforms into YbOF-t during the consecutive catalytic tests at 700 °C.

As noted in the Introduction, several fluorides have been used to promote the OCM activity of oxide-based catalysts. However, these earlier studies focused on surface modifications of the catalysts without substantially altering the atomic arrangement at the catalyst surface. In contrast, the present comprehensive study may shed light on intrinsic compositional/structural effects in oxyfluorides, compared to oxide-fluoride composites investigated previously. The five REOFs with RE = La, Sm, Eu, Dy, and Y show clearer catalytic activity trends than their corresponding REOs (Fig. 3). It is noteworthy that all REOFs, except for YbOF, are isostructural, whereas multiple structural types exist among the corresponding REOs. In the case of YbOF, the OCM behavior differs markedly between its two polymorphs. These findings suggest that both the crystallographic properties and the chemical nature of RE^{3+} ions are decisive factors governing OCM performance.

To gain deeper insights into the catalytic decisive factors of REOFs, their CO_2-TPD profiles were measured (Fig. 4 and Fig. S3). CO_2 desorption between 300 and 600 °C corresponds to moderate basic sites, which are reported to be associated with OCM selectivity.[37] Among the REOFs investigated, LaOF exhibits the largest quantity of moderate basic sites, whereas YOF and DyOF display only small amounts. When normalized by the specific surface area, the amount of moderate basic sites follows the order YOF ≈ DyOF < EuOF < SmOF < LaOF. Similarly, surface oxygen species have also been reported to influence OCM selectivity, with moderately bound oxygen species considered active in the reaction. As demonstrated in Fig. 5 and Fig. S4, O_2 desorption signals between 400 and 600 °C correspond to OCM-selective oxygen species.[37] LaOF, SmOF, and EuOF exhibit large amounts of moderately bound oxygen species, while YOF shows moderate levels. The normalized quantities follow the sequence DyOF < YOF < EuOF ≈ SmOF < LaOF. Notably, both sequences parallel the order of REOF lattice size (YOF < DyOF < EuOF < SmOF < LaOF), indicating that the ionic size of RE^{3+} influences the surface basicity and the stability of adsorbed oxygen species, thereby ultimately affecting the OCM catalytic activity.

Considering that oxide anions are stronger electron donors than fluoride anions, it can be inferred that oxide anions on REOF surfaces serve as the dominant basic sites responsible for methyl radical formation.[38] Therefore, the electron density at oxide anions can be directly correlated with the basicity strength of REOFs. Because fluorine is more electronegative than oxygen, fluoride anions in REOFs attract electrons more strongly than oxide anions, thereby reducing the electron density and weakening the basicity at the oxide anions. A similar observation has also been reported for Ba–Ce-based proton conductor, in which fluoride doping decreases oxide basicity.[39] The extent of electron withdrawal by fluoride anions depends on the RE–F bond length. In YOF, the shorter Y–F bond enhances electron attraction by fluoride, leading to lower electron density and weaker basicity at the oxide anions. In contrast, LaOF possesses longer La–F bonds, which diminish the electron-withdrawing effect of fluoride, thereby resulting in higher electron density at oxide anions and stronger basicity.

The same argument also applies to the trend in O_2 adsorption strength. On REOF surfaces, O_2 molecules may adsorb at cation sites or oxygen vacancies. Once adsorbed, O_2 can accept

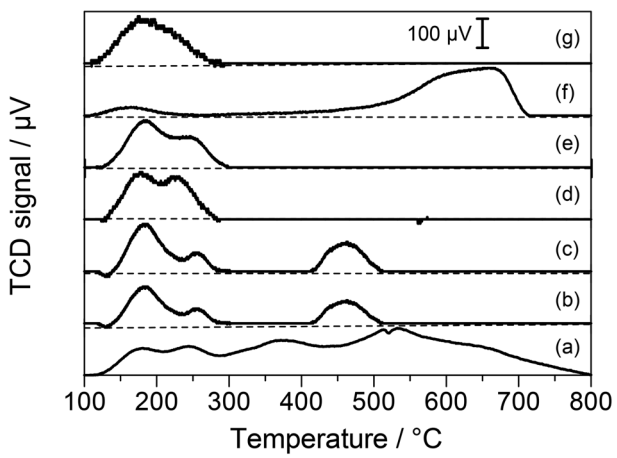

Fig. 4 CO_2-TPD profiles of (a) LaOF, (b) SmOF, (c) EuOF, (d) DyOF, (e) YOF, (f) YbOF-m, and (g) YbOF-t.

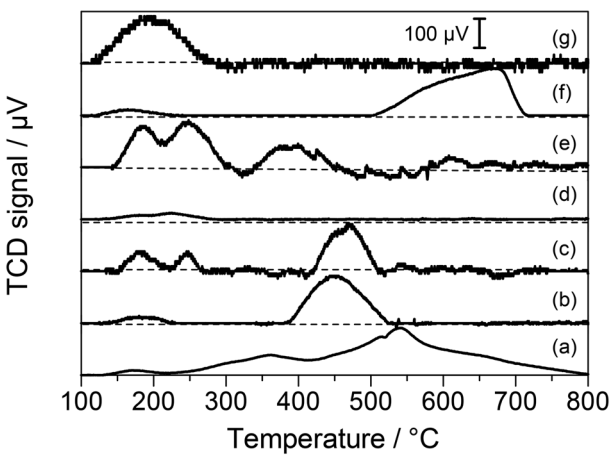

Fig. 5 O_2-TPD profiles of (a) LaOF, (b) SmOF, (c) EuOF, (d) DyOF, (e) YOF, (f) YbOF-m, and (g) YbOF-t.

electrons and either transform into oxyanions (O_2^-, O_2^{2-}, and O^-) or refill oxygen vacancies as lattice oxygen (O^{2-}), as represented in eqn (6).[40] As the adsorbed O_2 species accept more electrons, their character shifts from nucleophilic to increasingly electrophilic, thereby strengthening the adsorption. As discussed above, fluoride anions withdraw electrons more strongly in YOF owing to the shorter Y–F bond. Consequently, Y^{3+} exhibits a lower electron density and reduced electron-donating ability, which limits the formation of electrophilic oxygen species. In contrast, the longer La–F bond in LaOF weakens the electron-withdrawing effect, enabling higher electron density at La^{3+} and promoting the generation of electrophilic oxygen species.

$$\frac{1}{2}O_2 \rightleftharpoons \frac{1}{2}O_2^- \rightleftharpoons \frac{1}{2}O_2^{2-} \rightarrow O^- \rightleftharpoons O^{2-} \quad (6)$$

High quantities of moderate basic sites and moderately bound oxygen species are generally considered beneficial for enhancing OCM activity. However, the results of this study do not fully align with previous observations. LaOF surpasses the other REOFs (RE = Sm, Eu, Dy, and Y) in both basicity strength and the abundance of OCM selective oxygen species. At 600 °C, LaOF and YOF exhibit the highest and lowest C_2 selectivities, respectively (Fig. 3b), in good agreement with the prediction. In contrast, at 800 °C the trend reverses, with YOF showing the highest C_2 selectivity and LaOF the lowest. This result suggests that more weakly bound lattice oxygen in LaOF, due to a longer La–O bond relative to Y–O, is more prone to participate in direct methane oxidation, thereby promoting deep methane oxidation at elevated temperatures.

Previous mechanistic studies of OCM have revealed that methane activation into methyl radicals, generated *via* hydrogen abstraction by the surface oxygen species, is essential for selective C_2 formation.[41] In contrast, the generation of methoxy or formyl species leads to further oxidation to CO_x, thereby reducing C_2 selectivity.[42] Gas-phase methyl radicals couple to form C_2 species, whereas adsorbed methyl radicals may undergo subsequent dehydrogenation to form formyl species.[41,42] The high C_2 selectivity of 45.2% observed for YbOF-m at 700 °C indicates that this catalyst is highly effective in activating methane into methyl radicals while suppressing deep methane oxidation. One factor influencing methyl radical generation is the nature of the surface oxygen species. The O_2-TPD profile of YbOF-m (Fig. 5f) shows that the majority of surface oxygen species are strongly bound to the catalyst surface, effectively suppressing deep methane oxidation.[43] In contrast, weakly bound oxygen species dominate on the YbOF-t surface (Fig. 5g) and reduce C_2 selectivity.

Crystal polymorphism is known to influence material surface properties,[44] and the distinct OCM performances of YbOF-m and YbOF-t likely originate from differences in their surface characteristics. The O/F ratios, measured by SEM-EDS to be 0.94 and 0.67 for YbOF-m and YbOF-t, respectively, indicate that YbOF-m possesses a more oxygen-rich surface than YbOF-t. In other words, YbOF-m contains a larger number of surface oxide anions, which are favorable for the OCM performance. This interpretation is consistent with the higher basicity of YbOF-m relative to YbOF-t. A similar rationale may also be applicable for explaining the different catalytic behaviors of the other REOFs, which adopt a trigonal structure and therefore display varying surface activities. Nevertheless, a more in-depth investigation is required for a clearer understanding.

Conclusion

This work focuses on the structural characterization and catalytic activity of mixed-anion rare-earth oxyfluorides (REOFs; RE = La, Sm, Eu, Dy, Y, and Yb) in the oxidative coupling of methane (OCM). Based on previous findings that the incorporation of halide anions and their interactions with oxide anions can enhance OCM performance, the effects of fluoride anions on the crystal structure, surface properties, and OCM activity of REOFs were systematically investigated. All REOFs crystallize in a trigonal structure, except YbOF, which adopts either monoclinic (YbOF-m) or tetragonal (YbOF-t) polymorphs. Among the trigonal REOFs, the CH_4 conversion and C_2 selectivity at 600 and 800 °C exhibit systematic increasing or decreasing trends, with increasing ionic radii of the RE^{3+} cations. At 800 °C, YOF shows the highest CH_4 conversion and C_2 selectivity, surpassing those of the other trigonal REOFs and the corresponding oxide, Y_2O_3, with values of 24.8% and 44.9%, respectively. Across the REOFs series, the OCM activity, lattice size, surface basicity, and the density of moderately bound surface oxygen species follow similar trends, indicating correlations among these factors. In addition, YbOF-m exhibits superior CH_4 conversion and C_2 selectivity compared to its tetragonal polymorph. At 700 °C, the C_2 selectivities are 45.2% and 14.5% for the monoclinic and tetragonal phases, respectively, highlighting a decisive role of the crystal structure in determining the OCM performance of REOF catalysts.

Author contributions

M. S. and T. M. conceived and designed the study. A. P., T. K., K. O. and S. O. conducted the experiments and analyzed the data. A. P. wrote the original draft, and T. M. reviewed and edited the manuscript based on the suggestions and comments from S. I. and W. U. All authors approved the final version of the manuscript. T. M. secured funding. T. M. managed the project administration.

Conflicts of interest

There are no conflicts to declare.

Data availability

The data supporting this article have been included as part of the supplementary information (SI). Supplementary information is available. See DOI: https://doi.org/10.1039/d5dt02519b.

Acknowledgements

The authors gratefully acknowledge Mr Kaito Asaoka of Kanagawa University for his contributions to the synthesis and catalytic activity tests of the rare-earth oxyfluoride catalysts. This study was partly supported by JSPS KAKENHI Grant Number JP22H05143 (Transformative Research Area (A) "Supra-ceramics").

References

1 E. V. Kondratenko, T. Peppel, D. Seeburg, V. A. Kondratenko, N. Kalevaru, A. Martin and S. Wohlrab, *Catal. Sci. Technol.*, 2017, **7**, 366–381.
2 R. Franz, E. A. Uslamin and E. A. Pidko, *Mendeleev Commun.*, 2021, **31**, 584–592.
3 C. A. Ortiz-Bravo, C. A. Chagas and F. S. Toniolo, *J. Nat. Gas Sci. Eng.*, 2021, **96**, 104254.
4 R. Li, J. Wu, X. Zhao, S. Song, C. Jiang, C. Xiong, J. Ding, H. Wan and G. Guan, *Chem. Eng. J.*, 2024, **490**, 151528.
5 Z. C. Xu and E. D. Park, *Catalysts*, 2022, **12**, 314.
6 W. Xu, Z. Wang, C. Huang and X. Wang, *ChemCatChem*, 2024, **16**, e202400692.
7 S. A. Vali, A. A. Markeb, J. Moral-Vico, X. Font and A. Sánchez, *Nanomaterials*, 2023, **13**, 2754.
8 S. J. Han, T. G. Gebreyohannes, S. W. Lee, S. K. Kim, H. W. Kim, J. Shin and Y. T. Kim, *Mol. Catal.*, 2023, **535**, 112864.
9 P. Schwach, X. Pan and X. Bao, *Chem. Rev.*, 2017, **117**, 8497–8520.
10 H. R. Godini and M. M. Bhasin, *Molecules*, 2024, **29**, 4649.
11 Y. T. Chua, A. R. Mohamed and S. Bhatia, *Appl. Catal., A*, 2008, **343**, 142–148.
12 S. Arndt, T. Otremba, U. Simon, M. Yildiz, H. Schubert and R. Schomäcker, *Appl. Catal., A*, 2012, **425–426**, 53–61.
13 S. Sourav, R. R. Fushimi and I. E. Wachs, *Catal. Today*, 2025, **459**, 115426.
14 A. M. Maitra, I. Campbell and R. J. Tyler, *Appl. Catal., A*, 1992, **85**, 27–46.
15 F. Alahmadi, A. Bavykina, D. Poloneeva, A. Ramirez, R. Schucker and J. Gascon, *AIChE J.*, 2023, **69**, e17959.
16 R. C. Schucker, K. J. Derrickson, A. K. Ali and N. J. Caton, *Appl. Catal., A*, 2020, **607**, 117827.
17 V. R. Choudhary and V. H. Rane, *J. Catal.*, 1991, **130**, 411–422.
18 U. Zavyalova, M. Holena, R. Schlögl and M. Baerns, *ChemCatChem*, 2011, **3**, 1935–1947.
19 R. Xi, J. Xu, Y. Zhang, Z. Zhang, X. Xu, X. Fang and X. Wang, *Catal. Today*, 2021, **364**, 35–45.
20 J. Xu, R. Xi, Z. Zhang, Y. Zhang, X. Xu, X. Fang and X. Wang, *Catal. Today*, 2021, **374**, 29–37.
21 C. T. Au, K. D. Chen and C. F. Ng, *Appl. Catal., A*, 1998, **171**, 283–291.
22 C. T. Au, H. He, S. Y. Lai and C. F. Ng, *J. Catal.*, 1996, **159**, 280–287.
23 R. Q. Long and H. L. Wan, *Appl. Catal., A*, 1997, **159**, 45–58.
24 F. Cheng, J. Yang, L. Yan, J. Zhao, H. Zhao, H. Song and L. Chou, *React. Kinet., Mech. Catal.*, 2018, **125**, 675–688.
25 N. Hiyoshi and T. Ikeda, *Fuel Process. Technol.*, 2015, **133**, 29–34.
26 C. T. Au, Y. Q. Zhang, C. F. Ng and H. L. Wan, *Catal. Lett.*, 1994, **23**, 377–386.
27 L. Armelao, G. Bottaro, L. Bovo, C. Maccato, M. Pascolini, C. Sada, E. Soini and E. Tondello, *J. Phys. Chem. C*, 2009, **113**, 14429–14434.
28 S. Chong and B. J. Riley, *J. Nucl. Mater.*, 2022, **561**, 153538.
29 M. Momai, S. Tamura and N. Imanaka, *J. Ceram. Soc. Jpn.*, 2024, **132**, 55–57.
30 N. Nunotani, Z. Li and N. Imanaka, *Int. J. Appl. Ceram. Technol.*, 2022, **19**, 746–752.
31 N. Nunotani, S. Saeki, K. Matsuo and N. Imanaka, *Mater. Lett.*, 2020, **258**, 126802.
32 C. T. Au, Y. Q. Zhang, H. He, S. Y. Lai and C. F. Ng, *J. Catal.*, 1997, **167**, 354–363.
33 T. Matsumoto, M. Saito, S. Ishikawa, K. Fujii, M. Yashima, W. Ueda and T. Motohashi, *ChemCatChem*, 2020, **12**, 1968–1972.
34 S. Yang, A. Anderko, R. E. Riman and A. Navrotsky, *J. Am. Ceram. Soc.*, 2022, **105**, 1472–1480.
35 R. D. Shannon, *Acta Crystallogr., Sect. A*, 1976, **32**, 751–767.
36 A. F. Wells, *Structural Inorganic Chemistry*, Oxford University Press Inc., New York, 5th edn, 1984.
37 J. Xu, R. Xi, Y. Gong, X. Xu, Y. Liu, X. Zhong, X. Fang and X. Wang, *Inorg. Chem.*, 2022, **61**, 11419–11431.
38 H. A. Prescott, Z. J. Li, E. Kemnitz, J. Deutsch and H. Lieske, *J. Mater. Chem.*, 2005, **15**, 4616–4628.
39 H. Zhou, L. Dai, L. Jia, J. Zhu, Y. Li and L. Wang, *Int. J. Hydrogen Energy*, 2015, **40**, 8980–8988.
40 Y. Gambo, A. A. Jalil, S. Triwahyono and A. A. Abdulrasheed, *J. Ind. Eng. Chem.*, 2018, **59**, 218–229.
41 J. Sun, J. W. Thybaut and G. B. Marin, *Catal. Today*, 2008, **137**, 90–102.
42 P. N. Kechagiopoulos, J. W. Thybaut and G. B. Marin, *Ind. Eng. Chem. Res.*, 2014, **53**, 1825–1840.
43 T. Matsumoto, S. Ishikawa, M. Saito, W. Ueda and T. Motohashi, *Catal. Sci. Technol.*, 2022, **12**, 75–83.
44 S. Ding, J. Zhao and Q. Yu, *Catalysts*, 2019, **9**, 768.